JACS
JOURNAL OF THE AMERICAN CHEMICAL SOCIETY

ARTICLE

pubs.acs.org/JACS

The Short-Lived Signaling State of the Photoactive Yellow Protein Photoreceptor Revealed by Combined Structural Probes

Pradeep L. Ramachandran,[†] Janet E. Lovett,[‡,§] Patrick J. Carl,[⊥] Marco Cammarata,[∥] Jae Hyuk Lee,[¶] Yang Ouk Jung,[¶] Hyotcherl Ihee,[*,¶] Christiane R. Timmel,[‡] and Jasper J. van Thor[*,†,■]

[†]Laboratory of Molecular Biophysics, Department of Biochemistry, University of Oxford, South Parks Road, Oxford OX1 3QU, U.K.

[‡]Inorganic Chemistry Laboratory, Centre for Advanced Electron Spin Resonance, Department of Chemistry, University of Oxford, South Parks Road, Oxford OX1 3QR, U.K.

[§]EaStCHEM School of Chemistry, University of Edinburgh, Edinburgh EH9 3JJ, U.K.

[⊥]Bruker BioSpin GmbH, Silberstreifen 4, 76287 Rheinstetten, Germany

[∥]European Synchrotron Radiation Facility, Grenoble Cedex 38043, BP 220, France

[¶]Center for Time-Resolved Diffraction, Department of Chemistry, Graduate School of Nanosecience and Technology (WCU), KAIST, Daejeon 305-701, Republic of Korea

[■]Division of Molecular Biosciences, South Kensington Campus, Imperial College London, London SW7 2AZ, U.K.

Supporting Information

ABSTRACT: The signaling state of the photoactive yellow protein (PYP) photoreceptor is transiently developed via isomerization of its blue-light-absorbing chromophore. The associated structural rearrangements have large amplitude but, due to its transient nature and chemical exchange reactions that complicate NMR detection, its accurate three-dimensional structure in solution has been elusive. Here we report on direct structural observation of the transient signaling state by combining double electron electron resonance spectroscopy (DEER), NMR, and time-resolved pump−probe X-ray solution scattering (TR-SAXS/WAXS). Measurement of distance distributions for doubly spin-labeled photoreceptor constructs using DEER spectroscopy suggests that the signaling state is well ordered and shows that interspin-label distances change reversibly up to 19 Å upon illumination. The SAXS/WAXS difference signal for the signaling state relative to the ground state indicates the transient formation of an ordered and rearranged conformation, which has an increased radius of gyration, an increased maximum dimension, and a reduced excluded volume. Dynamical annealing calculations using the DEER derived long-range distance restraints in combination with short-range distance information from $^{1}H-^{15}N$ HSQC perturbation spectroscopy give strong indication for a rearrangement that places part of the N-terminal domain in contact with the exposed chromophore binding cleft while the terminal residues extend away from the core. Time-resolved global structural information from pump−probe TR-SAXS/WAXS data supports this conformation and allows subsequent structural refinement that includes the combined energy terms from DEER, NMR, and SAXS/WAXS together. The resulting ensemble simultaneously satisfies all restraints, and the inclusion of TR-SAXS/WAXS effectively reduces the uncertainty arising from the possible spin-label orientations. The observations are essentially compatible with reduced folding of the I_2' state (also referred to as the 'pB' state) that is widely reported, but indicates it to be relatively ordered and rearranged. Furthermore, there is direct evidence for the repositioning of the N-terminal region in the I_2' state, which is structurally modeled by dynamical annealing and refinement calculations.

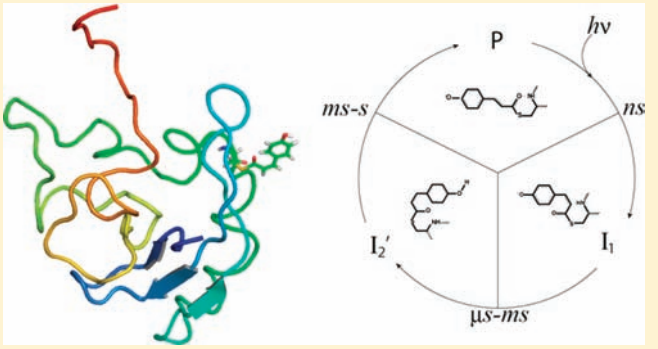

Photoreception is prevalent in all kingdoms of life and functions by linking the input signal, light, directly to structural and chemical processes. Resolving structural details of short-lived intermediates presents significant experimental challenges. Time-resolved protein crystallography[1−4] and pump−probe X-ray solution scattering[5−9] have provided important insight into light-activated structural dynamics. Because the structural dynamics in solution may be found to be fundamentally different from the crystalline state, techniques such as NMR and EPR may add essential structural information. Particularly, double electron electron resonance spectroscopy (DEER) is increasingly used to

Received: February 2, 2011
Published: May 31, 2011

dx.doi.org/10.1021/ja200617t | J. Am. Chem. Soc. 2011, 133, 9395–9404

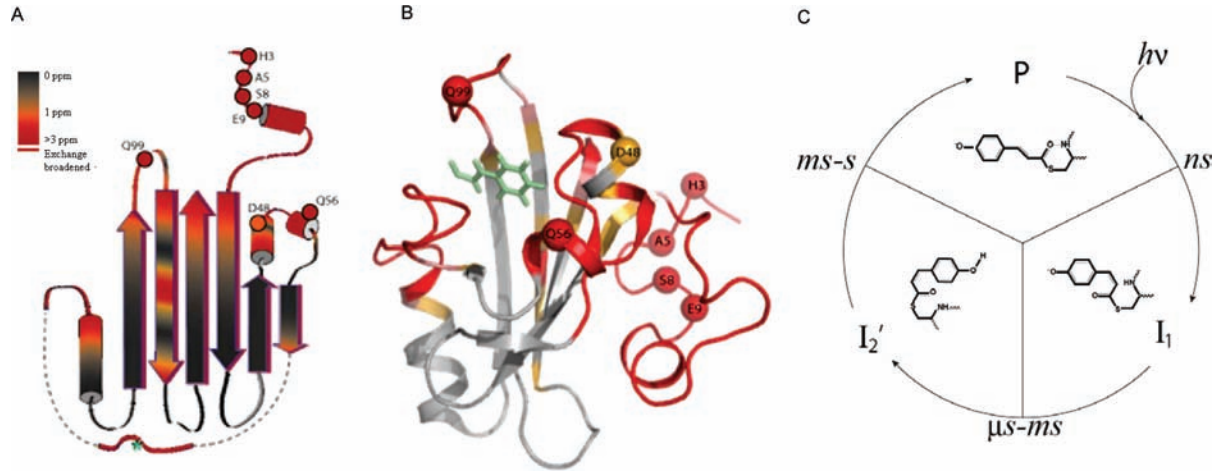

Figure 1. Topology cartoon representation of PYP and light-induced chemical shift perturbations. The color coding shows the chemical shift perturbation analysis of the I_2' state $^1H-^{15}N$ HSQC spectra of PYP relative to the ground state using $[(\Delta\sigma_{HN})^2 + (\Delta\sigma_N/6.515)^2]^{1/2}$, mapped on both 2D and 3D structure representation. Sites for spin-label attachment are indicated. A generalized and simplified photocycle scheme of PYP, including typical life times of intermediates and the structural states of the *p*-coumaric acid chromophore in the ground state (P) and intermediates, is shown. I_2' designates the metastable signaling intermediate of PYP that accumulates under continuous illumination.

probe biomolecular structure.[10−13] Extensive investigations have addressed the structural aspects of the signaling mechanism of the photoactive yellow protein (PYP) photoreceptor,[1−4,14−26] a 14.5 kDa cytoplasmic photoreceptor, considered to be responsible for the negative phototactic response of *Halorhodospira halophila*.[14] The transient structural changes that occur during its photocycle have been a focus of structural biology studies.[1−4,15−17] In contrast to the observations in the solution phase, structural changes in the crystalline state have smaller amplitudes because of molecular constriction.[1,3,18] Yet, the details of these structural rearrangements for the crucial intermediate in solution, the signaling state I_2' (also referred to as the 'pB' state) have remained unresolved. In solution, the I_2' state has the characteristics of a partially unfolded protein, as judged from NMR observables[17,19,20] [Figure 1A, and Figure S1 in Supporting Information (SI)], the loss of secondary structure elements observed by FTIR and CD spectroscopy,[18,21] time-resolved ORD spectroscopy[23] and altered hydrophobic dye binding and thermodynamic observables.[22,24,25] CD studies as well as stopped flow absorption spectroscopy have shown that the ground state recovery reaction matches folding reactions of the photoreceptor.[26] From NMR spectroscopy of I_2' a picture of a partially disordered state has emerged.[17,19,20] Particularly, nuclear Overhauser effect (NOE) data on the I_2' state of intact PYP were only observed for selected regions and exchange broadening led to the loss of many cross-peaks. Heteronuclear single quantum coherence (HSQC) perturbation spectroscopy and NOE measurements on a truncated mutant of PYP lacking the N-terminal 25 residues led to the calculation of structural ensembles that were characterized by the opening of the chromophore binding cleft and exhibited substantial disorder in the calculated ensemble that indicates low accuracy for parts of the polypeptide.[17,19] Both observations could be the result of force field parametrization in the absence of specific long-range distance information for regions that are characterized by exchange broadening. Results presented here are essentially in agreement with the first result supporting the global conformation from NMR,[17,19] but provide additional accuracy that reduces the root-mean-square (rms) displacements in calculated ensembles.

Here we use double electron electron resonance (DEER)[10−13] to obtain *long-range* distance information between selected sites within the protein (including the N-terminal domain) both in the ground state and photointermediate I_2' state. DEER is a 4-pulse EPR method (for details see Materials and Methods Summary and SI) that allows the determination of the distance, *r*, between two paramagnetic centers via the r^{-3} dependence of their mutual dipolar coupling. The success of this 4-pulse technique relies on the observation of an exploitable modulation pattern, namely a refocused echo recorded at one microwave frequency that must be modulated by application of a microwave pulse at a second frequency. The depth, frequency, and line shape of this modulation pattern can then be exploited to learn about the distance and distance distribution between the two paramagnetic sites. Here, we use the frequently employed method of site-directed mutagenesis to introduce paramagnetic centers in the form of spin labels into the otherwise entirely diamagnetic protein. We shall show that we observe distinct distances and distance distributions in these labeled protein mutants both in the ground and illuminated state, supporting the hypothesis that an ordered state is formed upon protein illumination.

Finally, we exploit small and wide-angle X-ray scattering (SAXS/WAXS) methods which, in solution, provide low- and intermediate-resolution information. Application of these techniques constitutes an additional, independent measurement of the global structure of the PYP I_2' intermediate in solution. The data obtained further strengthen the proposal of an illuminated state more structurally defined than assumed hitherto. The relative ordering of the I_2' structure does not refer to the folding of the polypeptide, but refers rather to the mean coordinate differences within the physical ensemble of the intermediate, and the results are consistent with the loss of secondary structure and additionally the NMR observables.

RESULTS

PYP Cysteine Mutants, NMR and Kinetic Analysis. In order to obtain the desired long-distance information using DEER

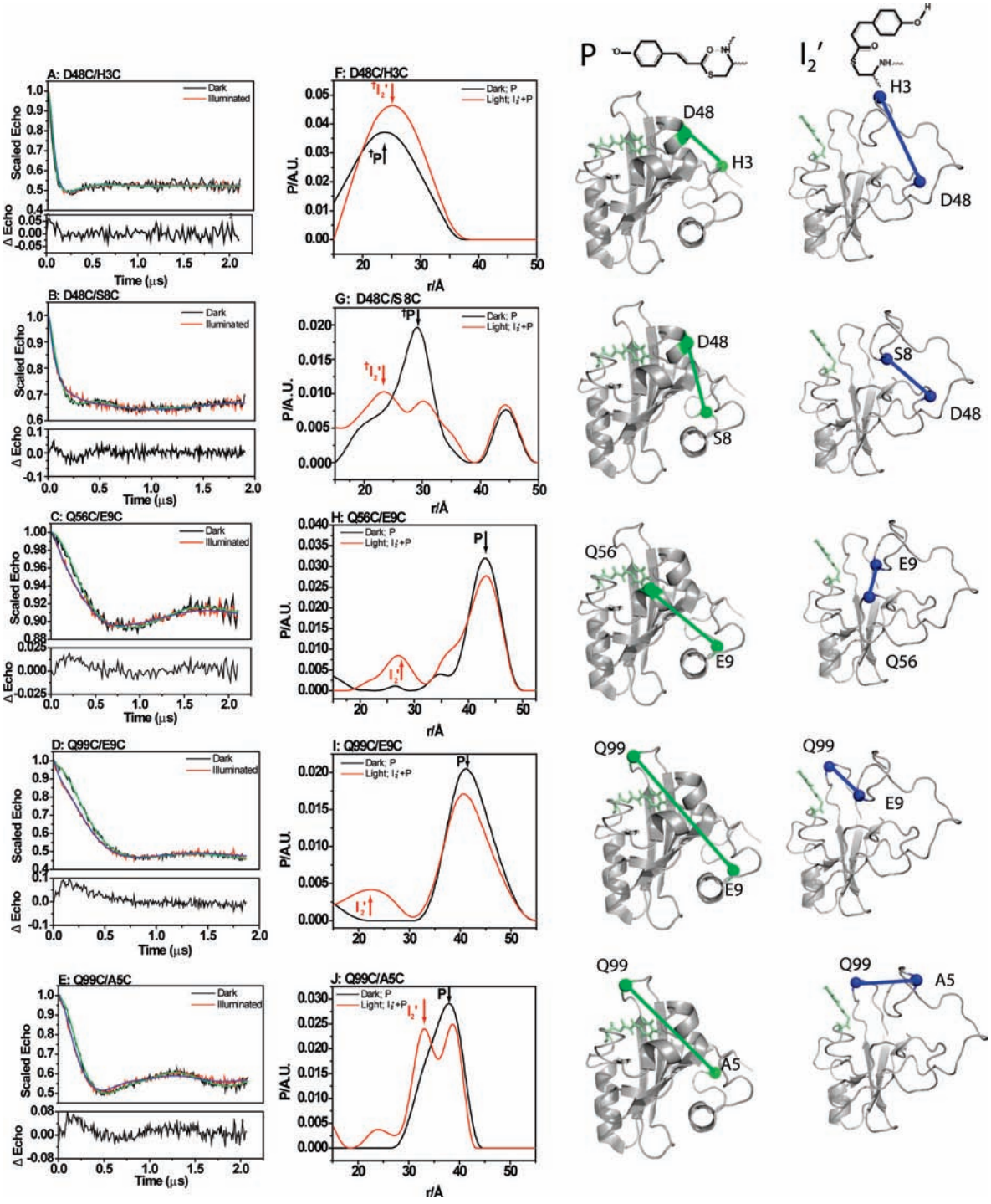

Figure 2. DEER echo decay data and simulations. (A−E) Experimental (background corrected, scaled) and simulated echo decay data of the five PYP mutants: D48C/H3C (A), D48C/S8C (B), Q56C/E9C (C), Q99C/E9C (D), and Q99C/A5C (E). Black and red lines show experimental data for dark and illuminated state, respectively. The light-induced differences (P *minus* I_2') are shown for each mutant below the respective scaled echo decay curves. Black and red graphs (panels F−J) are the corresponding distance distributions determined using Tikhonov regularization method in DeerAnalysis2006,[11] with the corresponding fits to the time domain traces (blue and green, panels A−E). Arrows in panels H−J indicate the distances assigned to the dark P state (dark; black) and I_2' intermediate (light; red) on the basis of the statistical χ^2 Gaussian calculations and the relative weights (Figure S11[SI]), that also closely correspond to the results from Tikhonov regularization (Table 1). In the case of D48C/H3C (panel F) and D48C/S8C (panel G), the arrows (including a dagger, †) indicate those corresponding to the maxima from Tikhonov regularization and their relative height only (Table 1). The distances in the P and I_2' states are indicated in representative structures (green and blue), where the coordinates for the I_2' structure are those determined from dynamical annealing calculations that use both DEER and NMR derived restraints. Regularization parameters for Tikhonov fits for F, G, H, and J was 100, and for I was 10. Samples contained 50 mM Tris-HCl, pH 7.0, 20% (v/v) glycerol and 75 μM protein double labeled with 1-oxyl-2,2,5,5-tetramethylpyrroline-3-methyl methane-thiosulfonate. DEER data were collected at 60 K.

dx.doi.org/10.1021/ja200617t |*J. Am. Chem. Soc.* 2011, 133, 9395–9404

Table 1. Results of Distance and Distance Distributions for P and I_2' from Tikhonov Regularization and χ^2 Gaussian Analysis[a]

	DEER: mean distance (Å) results from Tikhonov regularization; peaks assigned to I_2' or P based on relative weight.			DEER: mean distance/fwhm (Å) results from the best fit of the χ^2 Gaussian analysis; peaks assigned to I_2' or P based on relative weight.	
site pairs	P	I_2'	I_2' illuminated *minus* P (dark measurement) (Å)	P	I_2'
D48/H3	23.8	25.2	+1.4	N/A	N/A
D48/S8	29.8	23.2	−6.6	N/A[b]	N/A[b]
Q56/E9	43.0	27.2	−15.8	43.0/4.8	28.5/12.1
Q99/E9	40.9	21.9	−19.0	42.0/9.7	22.3/8.3
Q99/A5	38.9	33.5	−5.4	38.9/0.5	33.3/8.5

[a] Mean distances and distance distributions for the trapped ground state and I_2' intermediate populations with illumination determined by DEER, using both Tikhonov regularization (columns 2 and 3 for P and I_2' states) and χ^2 Gaussian analysis (columns 5 and 6 for P and I_2'); light-induced distance differences are relative to the ground-state measurements under dark conditions (Table S2 in SI). [b] For the D48C/S8C mutant, the analysis did show a significant difference between the DEER traces for the dark and irradiated samples, but the method could not unambiguously say what caused the difference in terms of distance shifts. In this case we included a third longer distance Gaussian distribution which we did not vary from the best fit value. As discussed in Supporting Information, the third distance was present due to the inclusion of the $(His)_6$-tag on this mutant. It had a mean at 4.45 nm, a fwhm 0.05 nm and a relative weight of 0.18.

spectroscopy (with a distance range of 20−80 Å), we created five fully photoactive double cysteine mutants (Figure 1A,B and Figure 2) of full length PYP.

The choice of mutation sites on the N-terminal domain and on either side of the chromophore binding cleft were guided by the DEER-accessible distance range, $^1H-^{15}N$ HSQC chemical shift perturbation analysis (Figure S1 in SI) as well as models for the I_2' state of N-terminally truncated PYP. For the latter, crucial structural information was lost due to exchange broadening in HSQC spectroscopy experiments (Figure 1A,B).[17,20]

Kinetic measurements acquired using transient absorption UV/visible spectroscopy indicated that the mutations decreased the P ground-state recovery rates and consequently allowed accumulation of experimentally observable levels of I_2' under continuous illumination for conducting DEER and NMR spectroscopy experiments (Table S1 in SI).

Light-induced $^1H-^{15}N$ HSQC chemical shift perturbation analysis of selected samples indicated that the photoaccumulated I_2' state corresponds well with time-resolved measurements of the I_2' state of the full length wild-type PYP[20] (Figure S1 in SI). Short-distance information from $^1H-^{15}N$ HSQC chemical shift perturbation analysis of the illuminated sample provided restraints for amides that have native-like contacts in the I_2' intermediate.[19] Using this procedure 46 out of 125 residues in the I_2' state were defined to have ground-state-like contacts, from which 275 native-like restraints were defined for the I_2' state that did not involve any for the 25 N-terminal residues (Figure S1 in SI). Selected $^1H-^{15}N$ cross-peaks present for the P ground state were not observed in the I_2' state due to exchange broadening, in agreement with previous observations[20] (SI, Table S4). Additional chemical shift based dihedral angle restraints[27] were defined for the P and I_2' states, respectively.

Double Electron Electron Resonance Spectroscopy. Panels A−E of Figure 2 display the dipolar evolution curves of the five doubly spin-labeled mutants of PYP in both the dark (black) and in the illuminated (red) state. Each subfigure also depicts the difference spectrum "dark − illuminated" in a bottom panel. As evidenced by the steeper initial gradient of the red (illuminated) modulation curve as compared to the dark (black) state and the resulting positive signal in the difference graph at short times, distances in the illuminated protein are, in general, shortened with respect to the dark state. Also displayed in A−E of Figure 2 are the Tikhonov-based simulations of the echo decay traces which provided very reasonable fits to the experimental data. F−J of Figure 2 display the distances obtained from the Tikhonov regularization fitting, where the peaks represent the best possible fits.

For all but the D48C/H3C mutant (Figure 2F), illumination of the protein causes a notable increase in the complexity of the distance distribution graphs with more pronounced populations at shorter distances, indicating the formation of a mixture of a cryo-trapped intermediate created by UV illumination, here tentatively hypothesized to be I_2', and P ground-state populations. The light-induced differences were reproducible, and multiple freeze−thaw cycles yielded identical results, recovering the ground state and producing the I_2' state repeatedly.

As the differences in the Tikhonov plots between illuminated and dark samples are small and in an attempt to quantify the difference between illuminated and dark DEER data, we performed the χ^2 analysis with Gaussian distributions as in refs 13 and 28 and as described in detail in the Materials and Methods and in further detail in the SI. As shown in the SI, we found that all samples except D48C/H3C exhibit statistically significant differences between the Gaussian distance distributions of the dark and illuminated forms. Further, the technique showed that the increased intensity of the shorter distance upon illumination was the main cause for the difference between the time traces for Q56C/E9C, Q99C/E9C and Q99C/A5C. In the case of the D48C/S8C sample a broader distribution for I_2' relative to the dark P state fitted the data better, consistent with the more pronounced modulation under dark conditions (Figure 2B, G). Distances for P were determined with highest accuracy for dark measurements (Figure 2F−J (black), Figure S11), while the distance for P in the illuminated mixture (Figure 2F−J (red)), present as a shoulder, were less well determined. Consequently, distances for P were taken from dark measurements (Table 1).

Therefore, for the Q56C/E9C, Q99C/E9C and Q99C/A5C samples the χ^2 Gaussian analysis support a relatively well-ordered I_2' state by comparing the full width at half-maximum (fwhm) values with those of the P state population (Table 1).

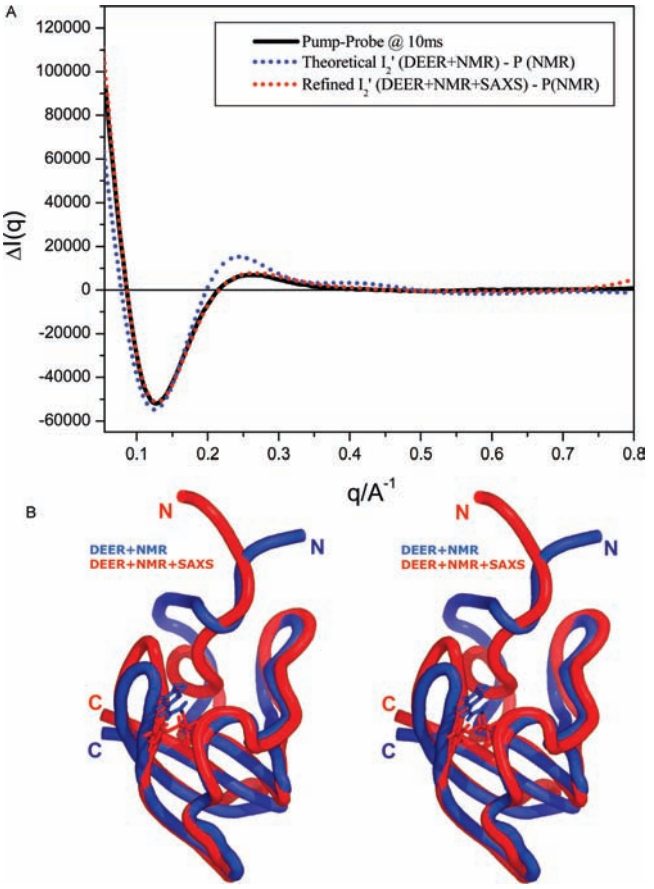

Figure 3. Time-resolved pump−probe SAXS/WAXS of full length wild-type PYP. (Black) Experimental pump-on minus pump-off difference X-ray scattering data on PYP as a function of q. The X-ray probe pulse is applied 10 ms after the 460 nm pump pulse that probes the I_2' transient population. PYP was at 4.4 mM concentration in Na-phosphate buffer pH 7, 20 mM NaCl at 293 K. (Blue) Theoretical difference scattering curve obtained using the DEER and NMR derived ensemble for the illuminated form and the previously determined NMR ensemble PDB 3PHY[29] for the ground state. The curve is obtained including a fitting of the density of the surface water layer in addition to intensity scaling for the I_2' state using CRYSOL.[31] (Red) Theoretical difference scattering curve obtained using the DEER, NMR and SAXS/WAXS derived ensemble for the illuminated form and the previously determined NMR ensemble PDB 3PHY for the ground state. The bottom panel shows a stereo image of the comparison of the average structures refined with DEER and NMR (blue) and combined DEER, SAXS/WAXS and NMR (red, PDB accession code: 2KX6) restraints simultaneously.

Possibly, an increased disorder could be the reason for the apparently broader distribution in the case of the D48C/S8C sample with illumination.

Time Resolved Pump−Probe X-ray Solution Scattering of the I_2' State at Small and Wide Angle (TR-SAXS/WAXS). In order to obtain further structural information on the I_2' state in solution, small and wide-angle X-ray scattering (SAXS/WAXS) was performed (see Materials and Methods of the SI). Calculations given in the SI indicate photolysis was saturating and conversion to I_2' was significant or complete in the interaction region (SI). Shown by the black solid line in Figure 3 are the experimentally obtained pump(on)−pump(off) difference data, $\Delta I(q)$ for a 10 ms delay from q = 0.05647−0.8 Å^{-1} (where $q = (4\pi \sin\theta)/\lambda$), corrected for a small background and temperature jump signal (SI). The shape of the graph shows clearly that the molecular scattering of the illuminated state (pump(on) signal) is characterized by increased scattering for small q value, and reduced scattering around q = 0.13 Å^{-1} as compared to the dark state. Smaller features are observed at higher resolution. The scattering data is indicative of an increased radius of gyration for the illuminated state, as well as an increased maximum diameter of the particle, that was also verified by ab initio shape reconstruction calculations (for more information, see SI).

Further, the increased zero-angle scattering intensity indicates a decreased excluded volume for the I_2' state, possibly indicating the formation of water-filled cavities not present in the P ground state. The scattering of the I_2' and P states corresponds closely with calculated scattering based on molecular models derived from NMR and DEER data (blue dotted graph in Figure 3), and in addition allowed structural refinement of the I_2' species by constructing a scattering curve for the pure species, as described below.

Structural Modeling Using Combined DEER, TR-SAXS/WAXS and NMR Data. Having measured the spin-label pair distances in both I_2' intermediate and P ground state, we proceeded to calculate structural ensembles using the long distance information from DEER analysis in combination with short distance restraints obtained from NMR spectroscopy as described in the Materials and Methods section (SI). The calculated ground-state structure was in close agreement with the NMR structure[29](PDB 3PHY) which supports that the freezing of the sample for DEER measurements does not perturb the structure within our resolution. Spin-label orientations were addressed by structure calculations using dynamic annealing[30] and previously reported restraints,[29] which included force field parametrized MTSSL pairs in individual runs (Figures 2 and 3).

For the I_2' intermediate, long-distance information from DEER experiments was combined with short distance information from ^{1}H−^{15}N HSQC chemical shift perturbation analysis and dihedral angle restraints.

Compared to the "open" conformation for the chromophore binding site in the illuminated protein obtained using only short-distance NMR derived restraints,[17] dynamical annealing calculations which take into account the additional long-distance DEER derived restraints suggest that the N-terminal domain has to rearrange and are additionally in agreement with an 'open' chromophore binding pocket.

A change in equilibrium dynamics in I_2' causes many ^{1}H−^{15}N HSQC cross-peaks to shift into the intermediate exchange regime. Due to chemical exchange reactions there are very few NOEs determined for the I_2' state even for well-defined HSQC cross peaks, and none are available to the N-terminal region. Structure solution therefore benefits from the addition of DEER spectroscopy that is insensitive to the change in equilibrium exchange kinetics. The power of DEER spectroscopy is to provide long-range energy terms specifically for those regions where no NMR data is available, which in this case directly support the 'open' conformation of the chromophore binding site. Calculated structures that have part of the N-terminal domain contacting the binding cleft simultaneously satisfy all DEER and NMR derived distance restraints (Figures 2 and 3). The resolution of the ensemble based on DEER and NMR measurements is relatively poor due to the possible spin-label orientations and restricted number of DEER restraints (see SI, Figure S6A).

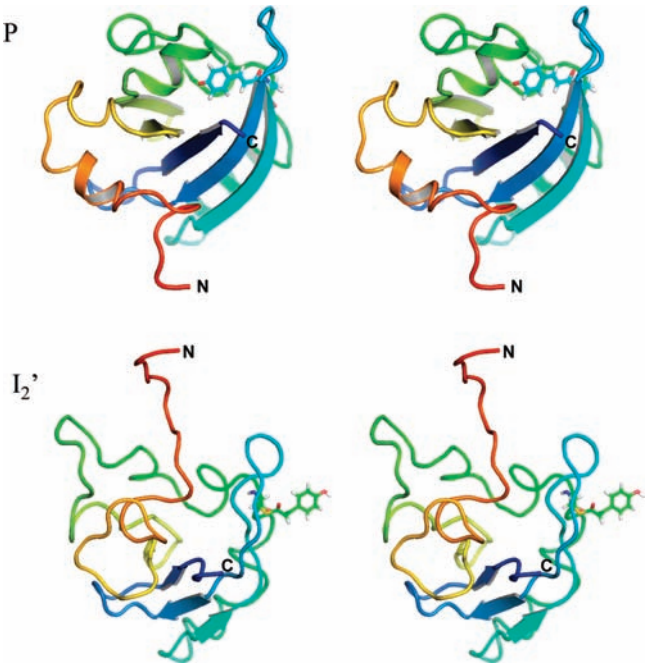

Figure 4. Comparison of the P ground state and the I_2' transient intermediate solution structure. Stereo figures of the ground-state structure P that satisfies dark NMR and DEER measurements are shown in the top panel. The bottom panel shows the resulting I_2' structure that satisfies DEER, SAXS/WAXS and NMR data simultaneously. The polypeptide is colored from red (N-terminus) to blue (C-terminus), to highlight the structural changes.

A theoretical difference X-ray scattering curve calculated for the DEER and NMR derived average structure (blue dotted curve, Figure 3A), that included fitting of the density of the surface water layer in addition to intensity scaling for the I_2' state using CRYSOL,[31] corresponds qualitatively with the experimental difference curve (Figure 3A; black solid curve). This indicates that the general shape changes observed in the NMR and DEER derived ensemble of the I_2' state are well supported by the TR-SAXS/WAXS measurements.

The structure was subsequently refined by including the experimental SAXS/WAXS data in the gradient for dynamical annealing calculations using code previously described.[32] In order to account for the possible spin-label orientations, (and because the TR-SAXS/WAXS samples used unlabeled wild-type PYP) we used two approaches. In the first approach, Cα−Cα distances were assumed to change upon illumination by the values that were determined for the inter-nitroxide distance changes (Table 1, column 4). In a second approach, Tyrosine side chains were modeled instead of nitroxides[12] (Figure S5 in SI). Both refinements resulted in structural ensembles that were structurally very similar (rmsd of 2.4 Å). These calculations took the DEER and NMR derived average structures, or any of the structures from the selected ensemble that are based on DEER and NMR data alone, as input. They were then stably refined over several cycles to converge to the surface water layer contrast value, and thus satisfied DEER, NMR, and SAXS/WAXS derived restraints simultaneously (Figure 3, dotted red curve). By adding low- and intermediate-resolution energy terms from SAXS/WAXS, essentially a subset of the DEER and NMR derived ensemble is selected, which increases the accuracy of the structure determination considerably (Figure S6 in SI).

DISCUSSION

This study unifies the extensive literature on the physical and structural properties of the I_2' intermediate. First, H/D exchange rate studies of the full length PYP showed the first 20 residues to be equally or possibly more protected in the I_2' state,[33] which provides an argument supporting the interaction of the N-terminus with the exposed chromophore binding region. Our results indicate that part of the N-terminal 20 residues, but not all, contact the exposed chromophore binding site (Figure 4). Furthermore, strong deprotection for residues 40−80 is consistent with the solvent exposed cavity that is formed in the I_2' ensemble (Figure S7 in SI). The role of the N-terminal residues is of particular interest. Smaller changes in heat capacity for the I_2' states of truncated mutants[34] and ground state recovery kinetics are incrementally reduced for larger N-terminal deletions.[37] These observations also indicate the involvement of the N-terminal region in the global structural changes in the I_2' state.

Second, the long distance restraints are consistent with a solvent-exposed cavity in the I_2' state, which could accommodate dye binding as observed in solution,[22,24] which was found to be specific for the I_2' state[35] and may explain its thermodynamic properties, specifically its heat capacity changes.[25] In addition, the light induced changes of the radius of gyration of the M100L mutant of the full length PYP as observed by small-angle X-ray scattering are 5%[36] and are also small for truncated variants.[37] Time-resolved diffusion constant measurement using the transient grating technique provided values of 1.27×10^{-10} m^2s^{-1} and 1.15×10^{-10} m^2s^{-1} for the ground state P and I_2' intermediate of the full length PYP at pH 8.0, showing a 10% increase in the hydrodynamic radius.[38] Single molecule studies have additionally shown that the PAS domain is extended by several nm in the I_2' state.[39]

This is in line with the calculated radii of gyration of the P and (DEER and NMR derived) I_2' structural ensembles which are 13.3 ± 0.08 Å and 15.4 ± 0.41 Å respectively. The fully refined DEER, SAXS/WAXS and NMR I_2' structure has a radius of gyration of 14.6 Å. Importantly, the fwhm values fitted to the DEER data do not support a fully extended and disordered structure of the N-terminus. Thus the structural model for the I_2' state shows substantial restructuring in solution relative to the ground state (Figure 4). These transitions are blocked in the crystalline environment,[1,15,18] and are likely to determine the interaction properties of the receptor in its signaling state under physiological conditions. The solution state I_2' structure substantially differs from the crystalline I_2' structure ('pB_2'),[1] however the structural change from P to I_2' in solution could be considered a larger amplitude motion than that is possible in the crystal, but having similar characteristics. Particularly, a clear progression of structural changes migrating toward the N-terminal region has been observed by X-ray crystallography, involving breakage of H-bonds and movements of the chromophore and key residues E46, Y42, N43, F28, L23, D24 and A44,[1,40] leading to a proposal for a helix-capping structural signaling model.[40] The formation of the solution state I_2' structure is blocked in the crystal[1,2,4] and it could be considered analogous as the structural successor of the crystalline I_2' state ('pB_2'),[1] in the cascading transformations.

The key observation of relatively narrow and accurately determined interspin distance distributions for the I_2' state in the DEER measurements shows that it has a well-defined structure. This should not be compared with the rms deviations in the calculated structural ensembles, that indicate inaccuracy of

Table 2. Structure Statistics for the I_2' State Intermediate Ensemble[a]

	DEER+NMR	DEER+NMR+SAXS/WAXS
Distance Restraints		
CSP-based native contacts	275	275
DEER derived	5	5
TALOS predicted dihedral	24	24
Violations (mean and s.d.)		
distance constraints, number (>0.5 Å)	0	1
dihedral angle constraints, number (>5°)	0	0
max. dihedral angle violation (deg)	0.34 ± 0.18	0.81 ± 0.04
max. distance constraint violation (Å)	0.03 ± 0.01	0.115 ± 0.001
Deviations from Idealized Geometry		
bond lengths (Å)	$0.01 \pm 1.70 \times 10^{-4}$	$1.34 \times 10^{-2} \pm 8.11 \times 10^{-5}$
bond angles (deg)	$1.22 \pm 3.16 \times 10^{-2}$	0.95 ± 0.01
impropers (deg)	$1.72 \pm 1.20 \times 10^{-1}$	0.63 ± 0.01
Average pairwise rmsd (Å)		
heavy	6.85 ± 1.61	1.39 ± 0.45
backbone	6.03 ± 1.73	1.13 ± 0.45
Ramachandran Analysis[b]		
favored regions (%)	71.31	45.1
additionally allowed regions (%)	95.9	73.0
disallowed regions (%)	4.1	27

[a] Calculations based on native contact and dihedral angle restraints and long distance restraints from DEER (left column), and additionally including SAXS/WAXS derived restraints (right column); results were also representative for calculations of the I_2' state that included parameterized MTSSL labels. [b] Ramachandran analysis was conducted on the calculated average structure from the ensemble using Molprobity (http://molprobity.biochem.duke.edu/).

structure determination that is more pronounced for parts that lack DEER derived restraints and thus effectively result from force field parametrization. In contrast, the overall rmsd for the fully refined DEER, SAXS/WAXS, and NMR I_2' structure is lower than that for the ground state NMR structure, which is a result of the increased number of fitting parameters with large force constants (Figure S6 in SI). Increased microscopic disorder is however present in I_2', which is observed from the decreased H/D exchange protection factors,[33] chemical exchange broadening in $^1H-^{15}N$ HSQC spectra[20] and altered ^{15}N relaxation rates.[17] These changes could arise primarily from frequency changes of the equilibrium fluctuations of the macromolecule, that also bring the chemical exchange rates near the chemical shift frequency differences, but the microscopic rms deviations do not necessarily have to be of higher magnitude in I_2' compared to the ground state. Additionally, the SAXS/WAXS data indicate no noticeable increase in disorder for I_2' from the distance distribution analysis and the constructed Kratky plot (SI Figure S13), which is in line with the DEER results. Importantly, our conclusions relate to the level of ordering rather than the state of folding of the I_2' intermediate, which is known to be reduced relative to that of the P ground state.

Environmental effects such as crystal packing, salt strength, solvent dielectric and pH are known to impact substantially on the structural transitions and photocycle kinetics of PYP.[41] Modification of the N-terminal region also has pronounced effects on both the photocycle kinetics as well as on the ordering of the I_2' structure, exemplified by an additional population with increased internitroxide distance in both P and I_2' states in experiments where an N-terminal $(His)_6$-tag was present (D48C/S8C mutant; Table 1), which also reduced the kinetics of P recovery. Thus, the results presented here are not necessarily directly comparable with those from other techniques that probe structural changes of PYP due to differences in the experimental conditions. DEER measurements were done at 60 K and with the addition of 20% glycerol, which affects the photocycle kinetics.[41] Illumination time was limited to several seconds in order to reduce potential accumulation of off-pathway products that have reduced recovery kinetics, whereas NMR spectroscopy was conducted under continuous illumination for longer time. Similarly, SAXS[37] and WAXS[42] experiments on the I_2' state are reported on truncated variants that lack parts of the N-terminus and may not necessarily undergo the same structural transitions as the full length or mutants of the full length used here. It is noted that a recent computational study aimed at the millisecond dynamics of PYP did not observe structural rearrangements to the extent that are observed in the experiments presented here.[43]

The calculated structural ensemble is fully and independently supported by DEER spectroscopy, by HSQC perturbation spectroscopy and by TR-SAXS/WAXS. No violations are present in the structural ensemble for DEER and NMR data, and a very close fit is obtained for the SAXS/WAXS data. Together they present strong evidence for the structural rearrangements but it should be stressed that it constitutes no proof of the structure solution being unique.

This work provides new structural information on the likely position of the N-terminal region as well as on global ordering parameters. Having performed direct transformation of experimental data from DEER and SAXS/WAXS we hypothesize that the I_2' state is likely to be well ordered. While DEER provides

long distance information, convoluted by possible different spin-label orientations, the TR-SAXS/WAXS provides low resolution global structural information on the entire polypeptide. Both indicate that no major differences in disorder occur in I_2' relative to P, and are compatible with the established view that the intermediate is less well folded.

Future paramagnetic relaxation enhancement measurements could potentially provide more NMR derived restraints since a number of the observable amides, with the exception of residues forming the loop region 84−87, fall between 10 and 35 Å of the paramagnetic center for all spin-labeled sites. We note that for the conditions used for DEER and NMR, an equilibrium exists between the I_2' state and its precursor I_2.[44] The I_2' state is associated with conformational changes and our analysis of NMR and DEER measurements in the photostationary state addresses two structural species where any possible accumulated I_2 state is interpreted to structurally resemble the ground state and the new population is assigned to the I_2' state.

CONCLUSIONS

Interspin Distance and Distance Distribution Changes in the I_2' State. From the described analysis procedures of the DEER data we conclude that for the Q56/E9, Q99/E9 and Q99/A5 mutants the χ^2 Gaussian analysis is able to provide further evidence that an additional species is present in the DEER data, which supports the Tikhonov regularisation results. This data fitting leads to strong evidence that light induced distance changes occur as indicated in column 4 of Table 1. The magnitude of the distance decreases between spin labels upon illumination, up to 19 Å, demonstrates that pronounced structural rearrangements occur upon formation of the photointermediate I_2'. The DEER spectroscopy measurements therefore indicate that the I_2' intermediate is well ordered and also should be relatively compact, with reduced distances between sites on the N-terminal domain (A5, S8, E9) and sites on either side of the chromophore binding cleft (D48, Q56, E99) (Figure 2). This general conclusion therefore provides new structural insight with regard to the intermediate's relatively well ordered state and the role of the N-terminus in the photocycle transitions. Previous work has indicated loss of α-helical content for the N-terminal region.[17−23] Our results are fully compatible with this view. Furthermore, part of the N terminus must extend away from the main core, as is evident from the increased D_{max} parameter (maximal dimension), which is also supported by the DEER results as well as the explicit structure calculations (Figures 3, 4).

The TR-SAXS/WAXS measurements fully support and are used to refine the structural models of the I_2' state and are in full agreement with the DEER derived conclusions with regard to its structural ordering (Table 2). This report is the first instance of structure solution of a transient intermediate using combined DEER, NMR and time-resolved SAXS/WAXS data. Recent success with combining NMR and SAXS/WAXS data for refining structural ensembles[32,45−47] has shown that inclusion of global restraints is functionally complementary and successful for NMR structure solution, and our work shows that pump−probe X-ray scattering measurements have decisive value for time-resolved structure determination when used in combination with additional experimental restraints from DEER and NMR.

MATERIALS AND METHODS SUMMARY

Full methods for spin labeling, four-pulse DEER EPR spectroscopy, time-resolved pump−probe X-ray scattering, NMR spectroscopy, and structural modeling accompany this manuscript in the SI.

NMR Spectroscopy. $^1H-^{15}N$ Heteronuclear NMR spectroscopy of the P and I_2' states of PYP mutants was performed on a Bruker Avance 500 spectrometer. PYP samples for NMR were 25 μM and 75 μM for A5C and Q56C, respectively, and contained 50 mM phosphate buffer, pH 5.75, 5% D_2O and a 5-fold molar excess of deuterated DTT. Photoaccumulation of the I_2' state was achieved with continuous blue-light illumination using an optical fiber. Experiments were conducted at 298 K. Assignments of cross-peaks for the P and I_2' states were obtained from refs 17, 20, and 29 Native contact restraints and dihedral angle restraints were generated for both P and I_2' using methods previously reported.[19]

Four Pulse DEER Spectroscopy. DEER spectroscopy of doubly spin-labeled samples at 60 K were performed on a Bruker ELEXSYS E580 spectrometer at X-band (9.5 GHz) frequency fitted with a 3 mm ER4118X-MS3 split-ring resonator using a $(\pi)/(2)-\tau_1-\pi-(\tau_1+t)-\pi_{pump}-(\tau_2-t)-\pi-\tau_2$ echo pulse sequence with 32 ns pulses at the observer frequency and a 12 ns pump frequency pulse. The frequency of the π_{pump} pulse was set to the maximum of the nitroxide echo detected field sweep spectrum and the observer frequency was offset by 65 MHz. A two-step phase cycle of the first observer pulse $(+x-x)$ with signal subtraction $(+s-s)$ was applied to correct for the receiver offsets. The time delays, τ_1 (200 ns), and τ_2 (2500 ns) were set to maximize signal-to-noise ratio and ensure proper collection of the dipolar time domain for the expected distances. The time, t, was incremented in either 8 or 16 ns steps, and hence, each time trace normally consisted of between 140 and 300 points.

Samples contained 50 mM Tris-HCl, pH 7.0, 20% (v/v) glycerol and 75 μM protein double labeled with 1-oxyl- 2,2,5,5-tetramethylpyrroline-3-methyl methane-thiosulfonate (MTSL, Toronto Research Chemicals). The I_2' state was photoaccumulated at room temperature under intense continuous illumination before rapid freezing in liquid nitrogen (under continued illumination).[2,41]

The analysis of DEER data was performed using two different approaches. First, Tikhonov regularization suitable for solving the ill-posed problem of determining a distance distribution directly from the DEER time traces without any prior assumptions on the form of the distribution was implemented in DeerAnalysis2006.[11] In the second approach (for short, the χ^2 method) the echo decay traces were fitted in the time domain with functions derived from Gaussian distances and distributions. The parameters were therefore mean and full width at half maximum (fwhm) for each Gaussian and a weighting factor. The two approaches are further detailed in the SI.

Time-Resolved Pump−Probe X-ray Scattering. Protocols for TR-WAXS data collection and data processing have been reported in detail elsewhere.[6] The experiment was performed in beamline ID09B of ESRF. Briefly, nanosecond pulsed optical excitation of a PYP sample in a capillary was combined with a pulsed X-ray probe at 18 KeV and 3.5% bandwidth. The delay was 10 ms after the UV excitation in order to target the transient population of the I_2' intermediate. Hoersch et al have shown that I_2 decays in about 2 ms to create the long-lived I_2' state.[48] Consequently, a delay of 10 ms selectively probes the I_2' state The pump-on and pump-off time-resolved X-ray scattering was recorded in 16 bunch mode and processed from q = 0.05647 to 0.8 Å^{-1} (where $q = (4\pi \sin \theta)/\lambda$ with 2θ and λ representing the scattering angle and the X-ray wavelength, respectively). The resulting difference data, $\Delta I(q)$, hence provide the I_2' minus P scattering signal.

Structural Modeling of the I_2' State in Solution. Initial structure calculations using NMR and DEER spectroscopy derived restraints were performed with CNS v1.1 using the RECOORDscripts.[49]

A torsion angle dynamics (TAD) annealing procedure was used which included: 10,000 steps at 10,000 K, followed by an 8000-step TAD cooling stage to a temperature of 2000 K. This was followed by a 10,000 step first Cartesian cooling stage to 1000 K and finally a 10,000 step second Cartesian cooling stage to 50 K. Structure refinements that simultaneously included DEER, NMR, and SAXS/WAXS data were done using a modified version of CNS as previously described.[32] The final refined ensemble has been submitted to the PDB database under accession code 2KX6.

■ ASSOCIATED CONTENT

Supporting Information. Nuclear magnetic resonance, double electron electron resonance, and small angle X-ray scattering tables; figures; and experimental details. This material is available free of charge via the Internet at http://pubs.acs.org.

■ AUTHOR INFORMATION

Corresponding Author
j.vanthor@imperial.ac.uk; hyotcherl.ihee@kaist.ac.kr

■ ACKNOWLEDGMENT

J.J.v.T. is a Royal Society University Research Fellow. We thank Gunnar Jeschke for help with initial experiments, for help with DEER data analysis and for valuable discussions. We thank Peter Höfer for access to facilities at Bruker BioSpin, Rheinstetten. We thank Jim McDonnell for help with acquiring NMR data. We acknowledge access to beamline ID09B at the European Synchrotron Radiation Facility under access number SC2438. We thank Michael Wulff for support at beamline ID09B at ESRF. We thank Jungkweon Choi for help with collecting TR-WAXS data. We thank Alexander Grishaev for help with the NIH CNS-SAXS program. J.J.v.T. is supported by the European Research Council via Grant Agreement No. 208650. J.E.L. is supported by EPSRC, University College, Oxford, and the Royal Society. This work was supported by Creative Research Initiatives (Center for Time-Resolved Diffraction) of MEST/NRF. J.H.L and Y.O.J acknowledge the support from the WCU program (R31-2008-000-10071-0).

■ REFERENCES

(1) Ihee, H.; Rajagopal, S.; Srajer, V.; Pahl, R.; Anderson, S.; Schmidt, M.; Schotte, F.; Anfinrud, P. A.; Wulff, M.; Moffat, K. *Proc. Natl. Acad. Sci. U.S.A.* **2005**, *102*, 7145.
(2) Moffat, K. *Nat. Struct. Biol.* **1998**, *5* (Suppl), 641.
(3) Perman, B.; Srajer, V.; Ren, Z.; Teng, T.; Pradervand, C.; Ursby, T.; Bourgeois, D.; Schotte, F.; Wulff, M.; Kort, R.; Hellingwerf, K.; Moffat, K. *Science* **1998**, *279*, 1946.
(4) Ren, Z.; Perman, B.; Srajer, V.; Teng, T. Y.; Pradervand, C.; Bourgeois, D.; Schotte, F.; Ursby, T.; Kort, R.; Wulff, M.; Moffat, K. *Biochemistry* **2001**, *40*, 13788.
(5) Ahn, S.; Kim, K. H.; Kim, Y.; Kim, J.; Ihee, H. *J. Phys. Chem. B* **2009**, *113*, 13131.
(6) Cammarata, M.; Levantino, M.; Schotte, F.; Anfinrud, P. A.; Ewald, F.; Choi, J.; Cupane, A.; Wulff, M.; Ihee, H. *Nat. Methods* **2008**, *5*, 881.
(7) Cho, H. S.; Dashdorj, N.; Schotte, F.; Graber, T.; Henning, R.; Anfinrud, P. *Proc. Natl. Acad. Sci. U.S.A.* **2010**, *107*, 7281.
(8) Ihee, H. *Acc. Chem. Res.* **2009**, *42*, 356.
(9) Kim, K. H.; Oang, K. Y.; Kim, J.; Lee, J. H.; Kim, Y.; Ihee, H. *Chem. Commun. (Camb)* **2011**, *47*, 289.
(10) Hubbell, W. L.; Cafiso, D. S.; Altenbach, C. *Nat. Struct. Biol.* **2000**, *7*, 735.
(11) Jeschke, G.; Chechik, V.; Ionita, P.; Godt, A.; Zimmermann, H.; Banham, J.; Timmel, C. R.; Hilger, D.; Jung, H. *Appl. Magn. Reson.* **2006**, *30*, 473.
(12) Jeschke, G.; Polyhach, Y. *Phys. Chem. Chem. Phys.* **2007**, *9*, 1895.
(13) Lovett, J. E.; Hoffmann, M.; Cnossen, A.; Shutter, A. T.; Hogben, H. J.; Warren, J. E.; Pascu, S. I.; Kay, C. W.; Timmel, C. R.; Anderson, H. L. *J. Am. Chem. Soc.* **2009**, *131*, 13852.
(14) Sprenger, W. W.; Hoff, W. D.; Armitage, J. P.; Hellingwerf, K. J. *J. Bacteriol.* **1993**, *175*, 3096.
(15) Genick, U. K.; Borgstahl, G. E.; Ng, K.; Ren, Z.; Pradervand, C.; Burke, P. M.; Srajer, V.; Teng, T. Y.; Schildkamp, W.; McRee, D. E.; Moffat, K.; Getzoff, E. D. *Science* **1997**, *275*, 1471.
(16) Genick, U. K.; Soltis, S. M.; Kuhn, P.; Canestrelli, I. L.; Getzoff, E. D. *Nature* **1998**, *392*, 206.
(17) Bernard, C.; Houben, K.; Derix, N. M.; Marks, D.; van der Horst, M. A.; Hellingwerf, K. J.; Boelens, R.; Kaptein, R.; van Nuland, N. A. *Structure* **2005**, *13*, 953.
(18) Xie, A.; Kelemen, L.; Hendriks, J.; White, B. J.; Hellingwerf, K. J.; Hoff, W. D. *Biochemistry* **2001**, *40*, 1510.
(19) Fuentes, G.; Nederveen, A. J.; Kaptein, R.; Boelens, R.; Bonvin, A. M. *J. Biomol. NMR* **2005**, *33*, 175.
(20) Rubinstenn, G.; Vuister, G. W.; Mulder, F. A.; Dux, P. E.; Boelens, R.; Hellingwerf, K. J.; Kaptein, R. *Nat. Struct. Biol.* **1998**, *5*, 568.
(21) Hoff, W. D.; Xie, A.; Van Stokkum, I. H.; Tang, X. J.; Gural, J.; Kroon, A. R.; Hellingwerf, K. J. *Biochemistry* **1999**, *38*, 1009.
(22) Lee, B. C.; Croonquist, P. A.; Sosnick, T. R.; Hoff, W. D. *J. Biol. Chem.* **2001**, *276*, 20821.
(23) Chen, E.; Gensch, T.; Gross, A. B.; Hendriks, J.; Hellingwerf, K. J.; Kliger, D. S. *Biochemistry* **2003**, *42*, 2062.
(24) Hendriks, J.; Gensch, T.; Hviid, L.; van Der Horst, M. A.; Hellingwerf, K. J.; van Thor, J. J. *Biophys. J.* **2002**, *82*, 1632.
(25) Van Brederode, M. E.; Hoff, W. D.; Van Stokkum, I. H.; Groot, M. L.; Hellingwerf, K. J. *Biophys. J.* **1996**, *71*, 365.
(26) Lee, B. C.; Pandit, A.; Croonquist, P. A.; Hoff, W. D. *Proc. Natl. Acad. Sci. U.S.A.* **2001**, *98*, 9062.
(27) Cornilescu, G.; Delaglio, F.; Bax, A. *J. Biomol. NMR* **1999**, *13*, 289.
(28) Bevington, P. R.; Robinson, D. K. *Data Reduction and Error Analysis for the Physical Sciences*, 2nd ed.; McGraw-Hill: Boston, 1992.
(29) Dux, P.; Rubinstenn, G.; Vuister, G. W.; Boelens, R.; Mulder, F. A.; Hard, K.; Hoff, W. D.; Kroon, A. R.; Crielaard, W.; Hellingwerf, K. J.; Kaptein, R. *Biochemistry* **1998**, *37*, 12689.
(30) Brunger, A. T.; Adams, P. D.; Clore, G. M.; DeLano, W. L.; Gros, P.; Grosse-Kunstleve, R. W.; Jiang, J. S.; Kuszewski, J.; Nilges, M.; Pannu, N. S.; Read, R. J.; Rice, L. M.; Simonson, T.; Warren, G. L. *Acta Crystallogr., Sect. D* **1998**, *54*, 905.
(31) Svergun, D. I.; Barberato, C.; Koch, M. H. J. *J. Appl. Crystallogr.* **1995**, *28*, 768.
(32) Grishaev, A.; Tugarinov, V.; Kay, L. E.; Trewhella, J.; Bax, A. *J. Biomol. NMR* **2008**, *40*, 95.
(33) Brudler, R.; Gessner, C. R.; Li, S.; Tyndall, S.; Getzoff, E. D.; Woods, V. L., Jr. *J. Mol. Biol.* **2006**, *363*, 148.
(34) van der Horst, M. A.; van Stokkum, I. H.; Crielaard, W.; Hellingwerf, K. J. *FEBS Lett.* **2001**, *497*, 26.
(35) Borucki, B.; Devanathan, S.; Otto, H.; Cusanovich, M. A.; Tollin, G.; Heyn, M. P. *Biochemistry* **2002**, *41*, 10026.
(36) Sasaki, J.; Kumauchi, M.; Hamada, N.; Oka, T.; Tokunaga, F. *Biochemistry* **2002**, *41*, 1915.
(37) Imamoto, Y.; Kamikubo, H.; Harigai, M.; Shimizu, N.; Kataoka, M. *Biochemistry* **2002**, *41*, 13595.
(38) Hoshihara, Y.; Imamoto, Y.; Kataoka, M.; Tokunaga, F.; Terazima, M. *Biophys. J.* **2008**, *94*, 2187.
(39) Zhao, J. M.; Lee, H.; Nome, R. A.; Majid, S.; Scherer, N. F.; Hoff, W. D. *Proc. Natl. Acad. Sci. U.S.A.* **2006**, *103*, 11561.
(40) Rajagopal, S.; Anderson, S.; Srajer, V.; Schmidt, M.; Pahl, R.; Moffat, K. *Structure* **2005**, *13*, 55.

(41) Meyer, T. E.; Tollin, G.; Hazzard, J. H.; Cusanovich, M. A. *Biophys. J.* **1989**, *56*, 559.
(42) Kamikubo, H.; Shimizu, N.; Harigai, M.; Yamazaki, Y.; Imamoto, Y.; Kataoka, M. *Biophys. J.* **2007**, *92*, 3633.
(43) Vreede, J.; Juraszek, J.; Bolhuis, P. G. *Proc. Natl. Acad. Sci. U.S.A.* **2010**, *107*, 2397.
(44) Borucki, B.; Joshi, C. P.; Otto, H.; Cusanovich, M. A.; Heyn, M. P. *Biophys. J.* **2006**, *91*, 2991.
(45) Schwieters, C. D.; Clore, G. M. *Biochemistry* **2007**, *46*, 1152.
(46) Xu, X.; Reinle, W.; Hannemann, F.; Konarev, P. V.; Svergun, D. I.; Bernhardt, R.; Ubbink, M. *J. Am. Chem. Soc.* **2008**, *130*, 6395.
(47) Zuo, X.; Wang, J.; Foster, T. R.; Schwieters, C. D.; Tiede, D. M.; Butcher, S. E.; Wang, Y. X. *J. Am. Chem. Soc.* **2008**, *130*, 3292.
(48) Hoersch, D.; Otto, H.; Joshi, C. P.; Borucki, B.; Cusanovich, M. A.; Heyn, M. P. *Biophys. J.* **2007**, *93*, 1687.
(49) Nederveen, A. J.; Doreleijers, J. F.; Vranken, W.; Miller, Z.; Spronk, C. A.; Nabuurs, S. B.; Guntert, P.; Livny, M.; Markley, J. L.; Nilges, M.; Ulrich, E. L.; Kaptein, R.; Bonvin, A. M. *Proteins* **2005**, *59*, 662.